


Photoelectron spectra in circularly and elliptically polarized laser pulses

Y. Gebre, S. Walker , and A. Becker 

JILA and Department of Physics, University of Colorado, Boulder, Colorado 80309-0440, USA

 (Received 14 August 2023; revised 26 December 2023; accepted 2 February 2024; published 27 February 2024)

We present results of numerical simulations of the time-dependent Schrödinger equation and theoretical analysis concerning the interaction of a rare gas atom with circularly and elliptically polarized laser pulses. In agreement with recent observation in circularly polarized fields, the photoelectron energy spectra for counterrotating electrons are peaked at lower kinetic energy than those for corotating electrons. We show that this difference can be interpreted as being due to the additional pathways to ionization that are available for the counterrotating electrons only. Furthermore, our results show, in agreement with earlier work, that the offset angle by which the emission of electrons is rotated in an elliptically polarized field increases with each successive above-threshold ionization (ATI) order and is larger for the emission from counterrotating states as compared to that from corotating states. A simple model based on the interference and relative phase difference between just three continuum states provides remarkable agreement and once again emphasizes the importance of the additional ionization pathways available for the counterrotating electrons.

DOI: [10.1103/PhysRevA.109.023120](https://doi.org/10.1103/PhysRevA.109.023120)

I. INTRODUCTION

Spin polarization of electrons is a valuable tool for probing the structure of and the electron dynamics in atoms, molecules, and solids. Spin-polarized photoelectrons can be generated via the interaction of atoms, molecules, or solids with circularly polarized laser light. An important aspect in the generation is the selective emission of electrons with a specific rotation in their initial state, which is determined by the magnetic quantum number of the state, relative to the helicity of the circularly polarized laser pulse. Numerous experimental and theoretical studies have recently analyzed how the helicity of the initial state impacts the electron emission in a strong laser field [1–57]. In the multiphoton and tunneling regime helicity-dependent ionization enhancement has been proposed [1] and observed [2,17,31], where counterrotating electrons from initial states with helicity opposite to the applied field are found to be preferentially ionized. This is in contrast to earlier findings for single-photon ionization, where the emission of electrons corotating with respect to the rotation of the applied electric field is more likely than that of counterrotating electrons [58–61].

Theoretical analysis, supported by numerical results of *ab initio* simulations of the time-dependent Schrödinger equation, indicate that the reversal in the ionization ratio of co- to counterrotating electrons as a function of wavelength is due to the photon absorption channels which are only accessible for electrons rotating opposite to the rotation direction of the external electric field [49,51]. This mechanism is illustrated in Fig. 1, which illustrates the absorption pathways for a right-handed circularly polarized field. Due to quantum selection rules the absorption of a photon causes a change in the orbital angular quantum number ($\Delta l = \pm 1$) and the magnetic quantum number ($\Delta m = +1$). Consequently, the available (real or virtual) states for the electron are constrained, as it transitions towards the continuum. For the counterrotating initial p state

($m_0 = -1, l_0 = 1$), the absorption of one photon leads to $m = 0$ and, hence, the electron can transition to either the $l = 0$ or $l = 2$ states. Conversely, for the corotating state ($m_0 = 1, l_0 = 1$), a transition occurs to the $m = 2$ state, which is available for the $l = 2$ state only. Thus, photoelectron emission from the counterrotating initial state benefits from the additional transition pathways during each successive photon absorption towards ionization. This results in the theoretically predicted and experimentally observed enhancement of ionization for counterrotating electrons in the few-photon, multiphoton, and tunneling regimes. The interpretation based on additional pathways and doorway states [49,51] has recently been reconfirmed in Ref. [56].

The goal of the present work is to study how these additional absorption pathways impact observables beyond the total ionization yields, such as photoelectron energy spectra and angular distributions. More specifically, we are interested in analyzing two recently reported observations. First, it has been shown that in circularly polarized laser fields the energy spectra of photoelectrons emitted from initial states with opposite helicity differ [5,14,17,31]. For counterrotating electrons the maximum of emission occurs at lower energies than for corotating electrons, which was related to the difference in azimuthal velocities at the tunneling exit. Photoelectrons with initial momentum antiparallel to the rotation of the field (i.e., counterrotating electrons) gain a lower final energy than those with parallel momentum (i.e., corotating electrons) [5,17].

Second, for ionization in elliptically polarized laser fields it has been found that the most probable emission angle, also called attoclock offset or streaking angle [62–66], increases with the energy of the emitted photoelectron [67–71]. This observation is in contrast to theoretical predictions based on classical Monte Carlo calculations due to which the Coulomb interaction of the photoelectron with the residual ion should lead to a decrease in the photoemission angle [67]. The results have been explained by a nonadiabatic tunneling effect

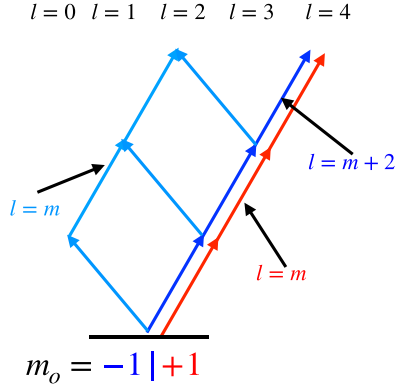


FIG. 1. Photon absorption pathways during the interaction of electrons in initial states with $m_0 = -1$ (counterrotating state) and $m_0 = 1$ (corotating state) with a right-handed circularly polarized pulse. Direct path for corotating electrons is indicated by the red arrows, direct path for counterrotating electrons is indicated by the blue arrows, and the offset path for counterrotating electrons is marked by the light blue arrows.

[1,72,73] in which the electron gains energy from the light field in the classically forbidden tunnel region, which impacts the tunnel exit position [67]. Concerning the relative helicity of the electrons with respect to the rotation direction of the applied field, the emission angle was found to be larger for the counterrotating electrons than for the corotating ones, which was again explained by the difference in lateral momentum of the two kinds of electrons at the tunneling exit [14].

In this study we aim to complement these previous findings and explanations by showing that the difference in the photoelectron energy spectra and the shifts in the emission angles can be understood based on quantum selection rules for photon absorption and the above-mentioned additional pathways for counterrotating electrons. To facilitate this analysis, we refer back to the diagram in Fig. 1 and introduce labels to distinguish the various pathways. The pathway with $\Delta l = +1$ (for right-handed circularly polarized light) in each absorption step is common for both the co- and the counterrotating initial state and we will refer to it as the “direct pathway.” The additional pathways, available for the counterrotating electrons only, in which in one absorption step $\Delta l = -1$, we label as “offset pathways.”

The rest of the paper is organized as follows: In the next section we briefly outline the details of the numerical calculations as well as the evaluation of the photoelectron energy and angular distributions from the numerical results. In Sec. III we present and discuss results for the energy spectra of electrons in circularly polarized field, while in Sec. IV we present numerical data and theoretical analysis for the most probable angular emission angle. The article ends with a brief summary.

II. NUMERICAL CALCULATIONS

We consider the interaction of a model neon atom in the single active electron approximation with an elliptically polarized intense laser pulse. The corresponding time-dependent Schrödinger equation (TDSE) in dipole approximation and velocity gauge is given by (we use Hartree atomic units

$e = m_e = \hbar = 1$, if not stated otherwise)

$$i \frac{\partial}{\partial t} \Psi(\mathbf{r}, t) = \left[-\frac{\nabla^2}{2} - \frac{i\mathbf{A}(t) \cdot \nabla}{c} + V_{SAE}(r) \right] \Psi(\mathbf{r}, t), \quad (1)$$

where $\mathbf{A}(t)$ is the vector potential of the laser pulse given by

$$\mathbf{A}(t) = A_0 \sin^2 \left(\frac{\pi t}{\tau} \right) [\sin(\omega t) \hat{\mathbf{x}} - \epsilon \cos(\omega t) \hat{\mathbf{y}}], \quad (2)$$

where ω is the laser frequency, $A_0 = \frac{c\sqrt{I}}{\omega}$, $\tau = \frac{2\pi N}{\omega}$, c is the speed of light, I is the peak intensity, and N denotes the number of cycles. Without loss of generalization, in our study we have chosen right-handed polarized pulses, i.e., $\epsilon > 0$ ($\epsilon = 1$ for circularly polarized light). The single-active-electron potential

$$V_{SAE}(r) = -\frac{1}{r} - \frac{9e^{-0.8870r}}{r} - 9.9286e^{-1.3746r} \quad (3)$$

$$+ 5.995e^{-3.79636r} \quad (4)$$

is fitted to a density functional theory calculation [74]. To solve the TDSE numerically we expand the wave function Ψ in spherical harmonics up to $l_{\max} = 60$ and $m_{\max} = 60$. The radius is discretized using the fourth-order finite difference method with a grid spacing of 0.05 a.u. and a maximum radius of 1250 a.u. with exterior complex scaling on the outer 62 a.u. of the grid. In time the wave function is propagated using the Crank-Nicolson method with a time step of 0.05 a.u. We have performed numerical calculations in which the central wavelength of the laser pulse is varied between 400 nm and 800 nm.

The energy-resolved photoelectron angular distributions can then be obtained from the time-propagated wave function as

$$F(\mathbf{k}) = |\langle \phi_{\mathbf{k}}^{(-)}(\mathbf{r}) | \Psi(\mathbf{r}) \rangle|^2 = \frac{1}{k^2} \left| \sum_{l,m} \left[(-i)^l e^{i\delta_{kl}} \int \chi_{kl}(r) \chi_{lm}(r) dr \right] Y_{l,m}(\hat{\mathbf{k}}) \right|^2, \quad (5)$$

where $\phi_{\mathbf{k}}^{(-)}(\mathbf{r}) = \frac{1}{k} \sum_{lm} i^l e^{-i\delta_l(k)} \frac{\chi_{kl}(r)}{r} Y_{lm}^*(\hat{\mathbf{k}}) Y_{lm}(\hat{\mathbf{r}})$ is the outgoing scattering state, $\Psi(\mathbf{r}) = \sum_{lm} \frac{\chi_{lm}(r)}{r} Y_{lm}(\hat{\mathbf{r}})$ is the wave function at the end of the pulse, $Y_{l,m}$ are the spherical harmonics, and δ_{kl} is the phase shift. To calculate the photoelectron energy spectrum, consisting of the above-threshold ionization (ATI) peaks, the summation is performed over the various orbital angular and magnetic components of the wave function. In certain parts of our analysis we will restrict the sum to show the impact of the different pathways on the results.

For the angular distributions we perform the sum across orbital angular and magnetic components of the wave function. We will consider angular emission patterns in the plane of polarization by setting $\theta = \pi/2$. In test calculations we have checked that the results are similar to those obtained after integration of the distribution over the angle θ . For the analysis we further consider the angular distribution corresponding to each individual ATI peak, which is determined by selecting a narrow energy bin around the position of each peak. Within this energy bin the sum across orbital angular and magnetic

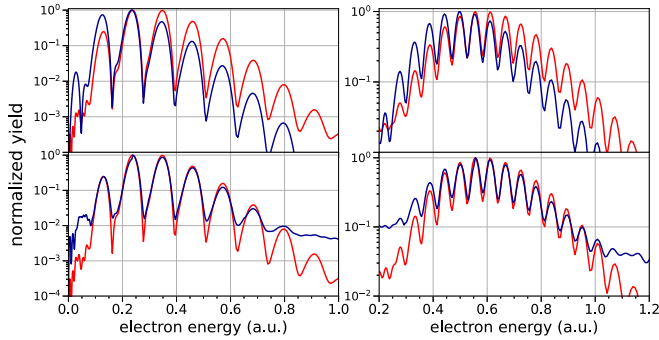


FIG. 2. Comparison of photoelectron energy spectra for a neon atom, initially in $l = 1, m = 1$ (corotating) state, indicated by the red curve, and atoms, initially in $l = 1, m = -1$ (counterrotating) state, indicated by the blue curve. The top panel represents the total spectrum, while the bottom panel shows the spectrum originating from the direct paths only. The results were obtained using a ten-cycle right-handed circularly polarized laser pulse with an intensity of $3 \times 10^{14} \text{ W/cm}^2$.

components of the wave function is being performed, which gives us the angular distribution specific to each ATI peak.

III. ENERGY SPECTRA IN CIRCULARLY POLARIZED PULSES

We have conducted simulations of the interaction between a model neon atom (in the single-active-electron approximation) and a right-handed circularly polarized laser pulse, considering the initial states of $l = 1, m = 1$ (corotating state, red line) and $l = 1, m = -1$ (counterrotating state, blue line). The pulse duration was set to ten cycles, wavelengths were 400 nm and 800 nm, and a peak intensity of $3 \times 10^{14} \text{ W/cm}^2$ was chosen. The results for the photoelectron energy spectra are shown in Fig. 2 for 400 nm (left column) and 800 nm (right column). In the top panels we show the comparison between the spectra for corotating (red line) and counterrotating (blue line) helicity of the initial state. For the comparison the highest ATI peak in each spectrum is set to 1. In agreement with earlier observations and studies [14,17,31], the shapes of the spectra differ for the emission from the two initial states. Furthermore, in agreement with the earlier predictions [14] the maximum in the spectrum for the counterrotating electrons occurs at lower energies than that for the corotating electrons. We may note that we did not include the contributions from the $m = 0$ state since those are negligible for the total yields.

In order to show that the difference in the spectra arises due to the additional offset pathway, available for the counterrotating electrons only, we note that the absorption of photons along the direct pathway is governed by quantum selection rules such that $l = m$ for corotating electrons and $l = m + 2$ in the case of counterrotating electrons (c.f. Fig. 1). Therefore, we have performed calculations in which we restricted the sum over orbital angular and magnetic components according to these rules when evaluating the energy spectra. The results are presented in the lower panels of Fig. 2 and, indeed, we observe a high degree of similarity in the spectra for co- and counterrotating electrons. The comparison shows that the discrepancy in the full spectra can be indeed attributed to the

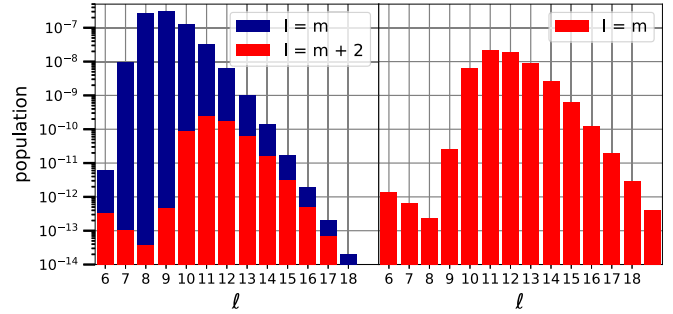


FIG. 3. Distribution of population in the orbital angular and magnetic states of a neon atom after interaction with a 400-nm circularly polarized laser pulse. Laser parameters are the same as in Fig. 2. Left for initial counterrotating state with $l = 1, m = -1$ and right for corotating state with $l = 1, m = 1$.

presence of the additional pathway exclusively available in the counterrotating case. To further interpret this result, we note that transitions into final states with small energies are more favored the lower the angular orbital momentum l [75]. Thus, for the counterrotating electrons transitions along the offset pathways (with $l = m$) result in stronger population of low-energy continuum states than photon absorption along the direct pathway (with $l = m + 2$), which explains the shift in the energy spectrum to lower energies.

We can gain more insight by investigating the population in the different orbital angular momentum (l) and magnetic (m) components of the continuum part of the time-propagated wave function. In Fig. 3 we present these components for the counter- (left column) and corotating (right column) initial states in the case of the TDSE simulation at 400 nm. We separate the components related to the direct pathway (shown in red) and those for the offset one (shown in blue). As expected from our analysis of the energy spectra, we see that the relative amount of population over the different components of l is similar for the direct pathway for both co- and counterrotating electrons. In contrast, those for the offset pathway have a different distribution. In particular, we note that for the counterrotating electrons the contributions related to the offset pathway are much stronger, reinforcing the interpretation that the additional pathway is the dominant one at this wavelength. Consequently, transitions via this pathway are the origin for the strong enhancement of the total ionization yield for counterrotating electrons, as discussed previously [49,51]. This can be further understood by the fact that along the offset pathway transitions occur between states having the same orbital angular and magnetic quantum number ($l = m$), which quantum mechanically have the strongest coupling.

Furthermore, the comparison in the left-hand panel of Fig. 3 shows that for the counterrotating state the distribution is peaked at lower orbital angular momentum for the offset pathway than for transitions via the direct pathway. To interpret this result we note that for a given initial state the final magnetic quantum number is determined by the number of photons, N_{phot} , absorbed by the electron ($N_{\text{phot}} = m - m_i$). On the one hand, the result is therefore in agreement with the analysis of the energy spectra, namely, that the shift to lower energies (corresponding to an absorption of a smaller number of photons) occurs for transitions along the offset pathway.

On the other hand, along the offset pathway the same magnetic quantum number (corresponding to the same number of absorbed photons) results in a lower orbital angular quantum number ($l = m$) than in the direct pathway ($l = m + 2$).

IV. ANGULAR DISTRIBUTIONS IN ELLIPTICALLY POLARIZED PULSES

We now turn to the angular distribution of the emitted electrons. For a circularly polarized pulse consisting of multiple cycles, emission is uniform across all angles within the plane of polarization. Instead, we focus on recent observations and predictions [14,67–71] for patterns in the angular distribution obtained in an elliptically polarized laser pulse with large ellipticity, close to circular polarization. Specifically, we will analyze the change in the most probable emission angle as a function of kinetic energy of the photoelectron and the difference in emission angle for counter- vs corotating electrons. To this end, we performed two sets of numerical simulations for the interaction of a neon atom with an elliptically polarized laser pulse, one for an initial (counterrotating) state of $l = 1, m = -1$ and another for a (corotating) state of $l = 1, m = 1$ for a 400-nm pulse with an ellipticity of 0.7. The results are illustrated in the top row of Fig. 4, where the results presented on the left correspond to the $l = 1, m = -1$ (counterrotating) case, and the results on the right represent the $l = 1, m = 1$ (corotating) case.

The angular emission patterns in the polarization plane (left column) show the expected ATI structure. The major axis of the polarization ellipse is oriented along the p_x axis. In agreement with recent observations [67], we observe that the angle of maximum emission, defined with respect to the minor x axis, increases as a function of the order of the ATI rings, for both co- and counterrotating electrons. This is seen even more clearly in the plots in the middle row of Fig. 4, where we present the angular distributions as a function of the offset angle for each ATI peak separately. We further observe, in agreement with earlier theoretical predictions [14], that the most probable emission angle for the counterrotating case is larger for each ATI peak and changes more significantly with each successive peak as compared to the corotating case. For pulses with polarization close to circular polarization, these findings are independent of the specific value of ellipticity. This can be seen from the results for the most probable emission angle as a function of ATI peak order in Fig. 5 for ellipticities of 0.8 (red symbols) and 0.9 (blue symbols).

Previous studies have indicated that the origin of the rotation is associated with nonadiabatic tunneling, where electrons acquire additional momentum in the parallel component during tunneling due to the interaction with the laser field [67,68]. Our goal is to provide complementary insight by exploring the correlation between the emission angle and the different orbital and magnetic state components that contribute to the photoelectron spectrum. To this end, we first identify the orbital angular momentum and magnetic states that provide the most significant contributions to the observed spectra. In both the corotating and counterrotating cases, we were able to identify three states that contribute most to each ATI peak. We plot the ATI-order resolved spectra produced by considering only these states in the bottom row of Fig. 4.

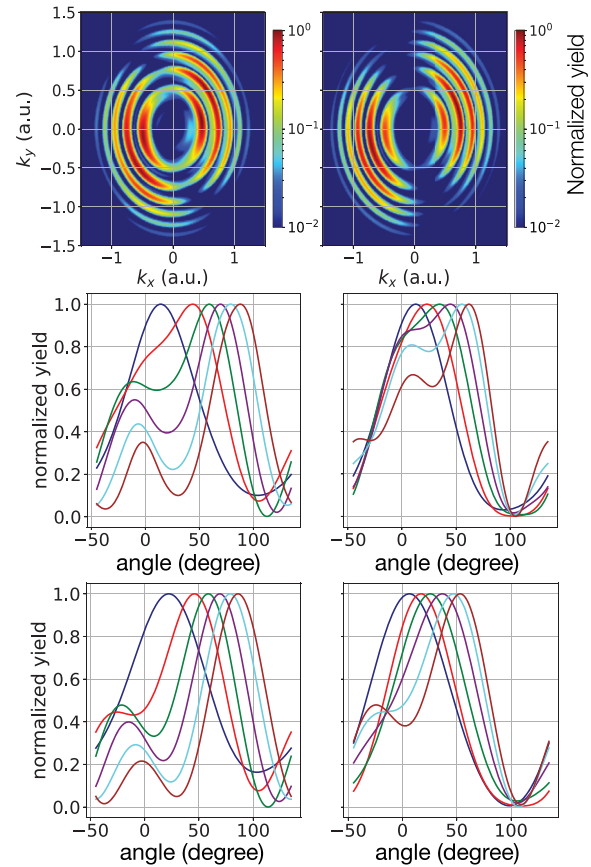


FIG. 4. Photoelectron spectrum for a neon atom interacting with an elliptically polarized laser pulse. The top row shows the angular distributions for the initial (counterrotating, left) state with $l = 1, m = -1$, and those for the initial (corotating, right) state with $l = 1, m = 1$. The plots in the middle row show the emission as a function of angle for each ATI peak, and those in the bottom row represent the spectra generated with the three highest contributing components. The pulse parameters are as follows: wavelength of 400 nm, intensity of 3×10^{14} W/cm², and ellipticity of 0.7.

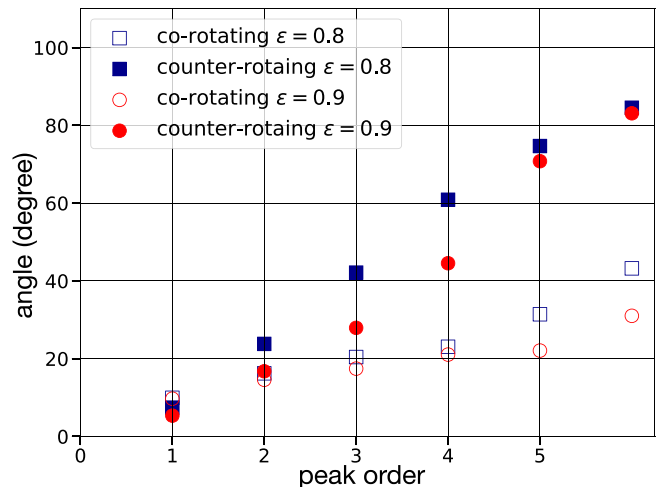


FIG. 5. The offset angle corresponding to the maximum emission of electrons for a neon atom interacting with an elliptically polarized pulse. The laser parameters are the same as in Fig. 4 for ellipticities of 0.8 (blue) and 0.9 (red).

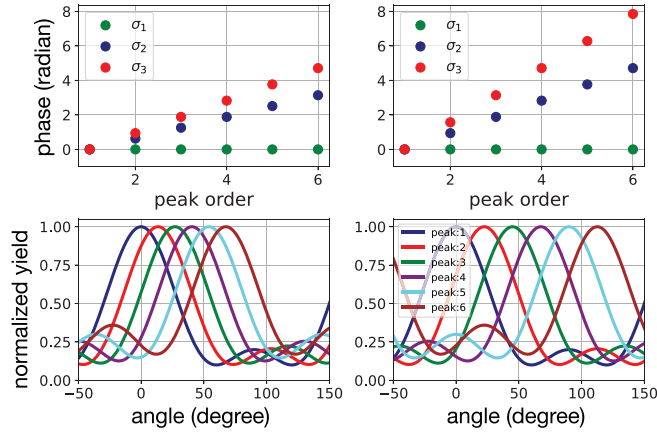


FIG. 6. Illustration of the dependence of angle of electron emission based on the model given by Eq. (6). Top panels show the phases of the three contributing components while the bottom panels show the resulting spectra.

Remarkably, we observe a highly accurate reproduction of the spectral features that we see in the full spectra (panels in the middle row).

Independent of the ATI order and for counter- as well as corotating initial states, we find that the three most contributing components for the n th ATI peak are represented by the quantum numbers $(l_n, m_n = l_n)$, $(l_n - 2, m_n - 2)$, and $(l_n - 4, m_n - 4)$, where $(l_n, m_n = l_n)$ is the state corresponding to the absorption of the minimum number of photons needed to ionize an electron with energy equal to that of the n th ATI peak. For the laser parameters used in the present TDSE calculations $l_n = n + 7$. Note that these channels are related to the offset (direct) pathway in the case of the counterrotating (corotating) electrons.

This identification simplifies the analysis significantly, as the spherical harmonics associated with the three states in the plane of polarization ($\theta = \frac{\pi}{2}$) can be expressed as $Y_{l,m=l} \propto e^{im\phi}$ and it can be assumed that interference and the phase difference between the states play a dominant role. To this end, we consider a simple model in which we express the spectrum for the n th peak as follows:

$$F_n \propto |e^{i\sigma_1} e^{im_n\phi} + e^{i\sigma_2} e^{i(m_n-2)\phi} + e^{i\sigma_3} e^{i(m_n-4)\phi}|^2, \quad (6)$$

where $e^{i\sigma_0}$ is the phase associated with the projection of the wave function on to the continuum states. To test this model, we set $\sigma_1 = 0$ and modify the relative phase between the states in Eq. (6) to study its impact on the change in the angle of maximum emission. The results in Fig. 6 confirm the expectations that the emission angle is determined by the relative phase of the different components.

We therefore proceed and extract from the TDSE simulations the relative phases of the three largest contributions in l and m for each ATI peak for both co- and counterrotating initial states. The results in Fig. 7 for ellipticities 0.7 (top row) and 0.8 (bottom row) indeed reveal the expected behavior. The relative phases increase for each successive ATI peak, which explains the increase in emission angle as a function of ATI order, and for each ATI peak the relative phases are larger in the case of the counterrotating state than for the corotating electrons.

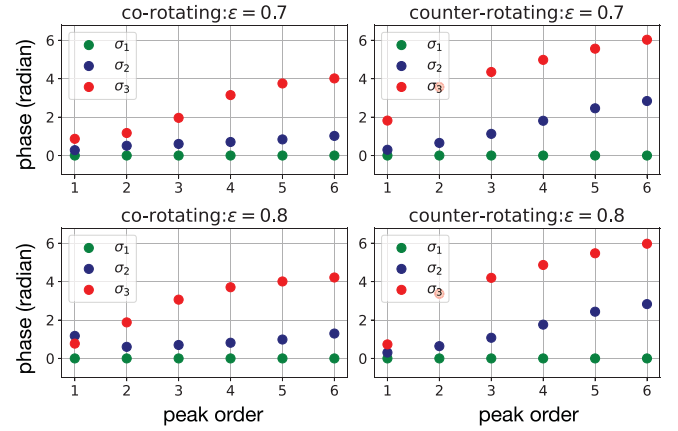


FIG. 7. Phases of the three biggest contributing components of the photoelectron spectrum of neon interacting with an elliptically polarized pulse, as extracted from the TDSE simulations. The plots on the left correspond to the corotating case, while the plots on the right correspond to the counterrotating case. The top row represents results from the interaction with a pulse having an ellipticity of 0.7, and the bottom row those for a pulse with an ellipticity of 0.8. Other laser parameters are as in Fig. 4.

V. SUMMARY

We have presented results of numerical simulations of the time-dependent Schrödinger equation for the interaction of a model neon atom in the single-active-electron approximation with circularly and elliptically polarized laser pulses. The results are found to be in agreement with recent observations and theoretical predictions. Complementary explanations based on the fact that counterrotating electrons can be emitted via additional pathways, as compared to their corotating counterparts, have been provided. Specifically, we have shown that the dominant ionization via these additional pathways leads to emission of photoelectrons at smaller kinetic energies in circularly polarized fields. Furthermore, in elliptically polarized laser pulses with large ellipticity the most probable emission angle is larger for counterrotating electrons and increases with each successive ATI order. Our analysis also shows that these two phenomena, which have previously been considered to be seemingly disparate, indeed have a shared underlying mechanism. In this context we may point out that the analysis and conclusions presented in this study depend on the angular momentum quantum number and not on the atomic potential. Those are therefore applicable for other atoms as well, including the hydrogen atom in its excited states.

ACKNOWLEDGMENTS

This work was primarily supported (Y.G., S.W., and A.B.) by a grant from the U.S. Department of Energy, Division of Chemical Sciences, Atomic, Molecular and Optical Sciences Program (Award No. DE-SC0001771). We also acknowledge the use of computing resources in part supported by a grant from the U.S. National Science Foundation (Grant No. PHY-1734006).

- [1] I. Barth and O. Smirnova, Nonadiabatic tunneling in circularly polarized laser fields: Physical picture and calculations, *Phys. Rev. A* **84**, 063415 (2011).
- [2] T. Herath, L. Yan, S. K. Lee, and W. Li, Strong-field ionization rate depends on the sign of the magnetic quantum number, *Phys. Rev. Lett.* **109**, 043004 (2012).
- [3] I. Barth and O. Smirnova, Nonadiabatic tunneling in circularly polarized laser fields. II. Derivation of formulas, *Phys. Rev. A* **87**, 013433 (2013).
- [4] I. A. Ivanov and A. S. Kheifets, Time delay in atomic photoionization with circularly polarized light, *Phys. Rev. A* **87**, 033407 (2013).
- [5] I. Barth and O. Smirnova, Comparison of theory and experiment for nonadiabatic tunneling in circularly polarized fields, *Phys. Rev. A* **87**, 065401 (2013).
- [6] I. Barth and O. Smirnova, Spin-polarized electrons produced by strong-field ionization, *Phys. Rev. A* **88**, 013401 (2013).
- [7] J. Kaushal and O. Smirnova, Nonadiabatic Coulomb effects in strong-field ionization in circularly polarized laser fields, *Phys. Rev. A* **88**, 013421 (2013).
- [8] I. Barth and O. Smirnova, Hole dynamics and spin currents after ionization in strong circularly polarized laser fields, *J. Phys. B: At. Mol. Opt. Phys.* **47**, 204020 (2014).
- [9] I. Barth and M. Lein, Numerical verification of the theory of nonadiabatic tunnel ionization in strong circularly polarized laser fields, *J. Phys. B: At. Mol. Opt. Phys.* **47**, 204016 (2014).
- [10] F. Mauger and A. D. Bandrauk, Electronic dynamics and frequency effects in circularly polarized strong-field physics, *J. Phys. B: At. Mol. Opt. Phys.* **47**, 191001 (2014).
- [11] J. H. Bauer, F. Mota-Furtado, P. F. O'Mahony, B. Piraux, and K. Warda, Ionization and excitation of the excited hydrogen atom in strong circularly polarized laser fields, *Phys. Rev. A* **90**, 063402 (2014).
- [12] T. Wang, X.-L. Ge, J. Guo, and X.-S. Liu, Sensitivity of strong-field double ionization to the initial ensembles in circularly polarized laser fields, *Phys. Rev. A* **90**, 033420 (2014).
- [13] J. Kaushal, F. Morales, L. Torlina, M. Ivanov, and O. Smirnova, Spin-orbit Larmor clock for ionization times in one-photon and strong-field regimes, *J. Phys. B: At. Mol. Opt. Phys.* **48**, 234002 (2015).
- [14] Y. Li, P. Lan, H. Xie, M. He, X. Zhu, Q. Zhang, and P. Lu, Nonadiabatic tunnel ionization in strong circularly polarized laser fields: Counterintuitive angular shifts in the photoelectron momentum distribution, *Opt. Express* **23**, 28801 (2015).
- [15] J. Kaushal, F. Morales, and O. Smirnova, Opportunities for detecting ring currents using an attoclock setup, *Phys. Rev. A* **92**, 063405 (2015).
- [16] M. Yuan, G. Zhao, and H. Liu, Influence of wavelength on nonadiabatic effects in circularly polarized strong-field ionization, *Phys. Rev. A* **92**, 053405 (2015).
- [17] A. Hartung, F. Morales, M. Kunitski, K. Henrichs, A. Laucke, M. Richter, T. Jahnke, A. Kalinin, M. Schöffler, L. Ph. H. Schmidt, M. Ivanov, O. Smirnova, and R. Dörner, Electron spin polarization in strong-field ionization of xenon atoms, *Nat. Photonics* **10**, 526 (2016).
- [18] X. Zhu, P. Lan, K. Liu, Y. Li, X. Liu, Q. Zhang, I. Barth, and P. Lu, Helicity sensitive enhancement of strong-field ionization in circularly polarized laser fields, *Opt. Express* **24**, 4196 (2016).
- [19] K. Liu and I. Barth, Nonadiabatic tunnel ionization of current-carrying orbitals of prealigned linear molecules in strong circularly polarized laser fields, *Phys. Rev. A* **94**, 043402 (2016).
- [20] D. B. Milošević, Possibility of introducing spin into attoscience with spin-polarized electrons produced by a bichromatic circularly polarized laser field, *Phys. Rev. A* **93**, 051402(R) (2016).
- [21] J. Wätzel and J. Berakdar, Discerning on a sub-optical-wavelength the attosecond time delays in electron emission from magnetic sublevels by optical vortices, *Phys. Rev. A* **94**, 033414 (2016).
- [22] M. Ilchen, N. Douguet, T. Mazza, A. J. Rafipoor, C. Callegari, P. Finetti, O. Plekan, K. C. Prince, A. Demidovich, C. Grazioli, L. Avaldi, P. Bolognesi, M. Coreno, M. Di Fraia, M. Devetta, Y. Ovcharenko, S. Düsterer, K. Ueda, K. Bartschat, A. N. Grum-Grzhimailo *et al.*, Circular dichroism in multiphoton ionization of resonantly excited He⁺ ions, *Phys. Rev. Lett.* **118**, 013002 (2017).
- [23] K. Liu and I. Barth, Spin-polarized photoelectrons produced by strong-field ionization of randomly aligned nitric oxide, *J. Mod. Opt.* **64**, 987 (2017).
- [24] K. Liu, K. Renziehausen, and I. Barth, Producing spin-polarized photoelectrons by using the momentum gate in strong-field ionization experiments, *Phys. Rev. A* **95**, 063410 (2017).
- [25] J. P. Wang and F. He, Tunneling ionization of neon atoms carrying different orbital angular momenta in strong laser fields, *Phys. Rev. A* **95**, 043420 (2017).
- [26] D. Ayuso, A. Jiménez-Galán, F. Morales, M. Ivanov, and O. Smirnova, Attosecond control of spin polarization in electron-ion recollision driven by intense tailored fields, *New J. Phys.* **19**, 073007 (2017).
- [27] M. M. Liu, M. Li, Y. Shao, M. Han, Q. Gong, and Y. Liu, Effects of orbital and Coulomb potential in strong-field nonadiabatic tunneling ionization of atoms, *Phys. Rev. A* **96**, 043410 (2017).
- [28] Q. Zhang, G. Basnayake, A. Winney, Y. F. Lin, D. Debrah, S. K. Lee, and W. Li, Orbital-resolved nonadiabatic tunneling ionization, *Phys. Rev. A* **96**, 023422 (2017).
- [29] S. Eckart, M. Kunitski, M. Richter, A. Hartung, J. Rist, F. Trinter, K. Fehre, N. Schlott, K. Henrichs, L. Ph. H. Schmidt, T. Jahnke, M. Schöffler, K. Liu, I. Barth, J. Kaushal, F. Morales, M. Ivanov, O. Smirnova, and R. Dörner, Ultrafast preparation and detection of ring currents in single atoms, *Nat. Phys.* **14**, 701 (2018).
- [30] S. Eckart, K. Fehre, N. Eicke, A. Hartung, J. Rist, D. Trabert, N. Strenger, A. Pier, L. Ph. H. Schmidt, T. Jahnke, M. S. Schöffler, M. Lein, M. Kunitski, and R. Dörner, Direct experimental access to the nonadiabatic initial momentum offset upon tunnel ionization, *Phys. Rev. Lett.* **121**, 163202 (2018).
- [31] D. Trabert, A. Hartung, S. Eckart, F. Trinter, A. Kalinin, M. Schöffler, L. Ph. H. Schmidt, T. Jahnke, M. Kunitski, and R. Dörner, Spin and angular momentum in strong-field ionization, *Phys. Rev. Lett.* **120**, 043202 (2018).
- [32] M. M. Liu, Y. Shao, M. Han, P. Ge, Y. Deng, C. Wu, Q. Gong, and Y. Liu, Energy- and momentum-resolved photoelectron spin polarization in multiphoton ionization of Xe by circularly polarized fields, *Phys. Rev. Lett.* **120**, 043201 (2018).
- [33] J. Kaushal and O. Smirnova, Looking inside the tunnelling barrier: I. Strong field ionisation from orbitals with high angular

- momentum in circularly polarised fields, *J. Phys. B: At. Mol. Opt. Phys.* **51**, 174001 (2018).
- [34] J. Kaushal and O. Smirnova, Looking inside the tunnelling barrier: II. Co- and counter-rotating electrons at the “tunnelling exit”, *J. Phys. B: At. Mol. Opt. Phys.* **51**, 174002 (2018).
- [35] D. D. A. Clarke, G. S. J. Armstrong, A. C. Brown, and H. W. van der Hart, R-matrix-with-time-dependence theory for ultrafast atomic processes in arbitrary light fields, *Phys. Rev. A* **98**, 053442 (2018).
- [36] K. Liu, H. Ni, K. Renziehausen, J. M. Rost, and I. Barth, Deformation of atomic p_{\pm} orbitals in strong elliptically polarized laser fields: Ionization time drifts and spatial photoelectron separation, *Phys. Rev. Lett.* **121**, 203201 (2018).
- [37] S.-D. Jheng, T.-F. Jiang, J.-H. Chen, and J.-L. Liu, Magnetic quantum number dependence of hydrogen photoelectron spectra under circularly polarized pulse in barrier suppression ionization regime, *Phys. Scr.* **93**, 085401 (2018).
- [38] M. Han, P. Ge, M.-M. Liu, Q. Gong, and Y. Liu, Spatially and temporally controlling electron spin polarization in strong-field ionization using orthogonal two-color laser fields, *Phys. Rev. A* **99**, 023404 (2019).
- [39] G. S. J. Armstrong, D. D. A. Clarke, A. C. Brown, and H. W. van der Hart, Electron rotational asymmetry in strong-field photodetachment from F^{-} by circularly polarized laser pulses, *Phys. Rev. A* **99**, 023429 (2019).
- [40] J. Hofbrucker, A. V. Volotka, and S. Fritzsche, Fluorescence polarization as a precise tool for understanding nonsequential many-photon ionization, *Phys. Rev. A* **100**, 011401(R) (2019).
- [41] S. Xu, Q. Zhang, X. Fu, X. Huang, X. Han, M. Li, W. Cao, and P. Lu, Towards atom-scale spin-selective electron emitters based on strong-field Freeman resonant ionization, *Phys. Rev. A* **102**, 063128 (2020).
- [42] D. Wu, F.-M. Guo, J.-G. Chen, J. Wang, and Y.-J. Yang, Ionization of an atom with different initial angular momenta in an intense circular polarized laser field, *J. Phys. B: At. Mol. Opt. Phys.* **53**, 235601 (2020).
- [43] J. H. Bauer and Z. Walczak, Ionization and excitation of low-lying circular states of the hydrogen atom in strong circularly polarized laser fields, *Phys. Rev. A* **101**, 063409 (2020).
- [44] G. S. J. Armstrong, D. D. A. Clarke, J. Benda, A. C. Brown, and H. W. van der Hart, Electron correlation and short-range dynamics in attosecond angular streaking, *Phys. Rev. A* **101**, 041401(R) (2020).
- [45] E. V. Gryzlova, M. M. Popova, and A. N. Grum-Grzhimailo, Spin polarization of photoelectrons in bichromatic extreme-ultraviolet atomic ionization, *Phys. Rev. A* **102**, 053116 (2020).
- [46] B. Böning, P. Abele, W. Paufler, and S. Fritzsche, A strong-field approach with realistic wave functions to the above-threshold ionization of Ba^{+} , *J. Phys. B: At. Mol. Opt. Phys.* **54**, 025602 (2021).
- [47] A. H. N. C. De Silva, D. Atri-Schuller, S. Dubey, B. P. Acharya, K. L. Romans, K. Foster, O. Russ, K. Compton, C. Rischbieter, N. Douguet, K. Bartschat, and D. Fischer, Using circular dichroism to control energy transfer in multiphoton ionization, *Phys. Rev. Lett.* **126**, 023201 (2021).
- [48] A. H. N. C. De Silva, T. Moon, K. L. Romans, B. P. Acharya, S. Dubey, K. Foster, O. Russ, C. Rischbieter, N. Douguet, K. Bartschat, and D. Fischer, Circular dichroism in atomic resonance-enhanced few-photon ionization, *Phys. Rev. A* **103**, 053125 (2021).
- [49] S. Walker, L. Kolanz, J. Venzke, and A. Becker, Enhanced ionization of counter-rotating electrons via doorway states in ultrashort circularly polarized laser pulses, *Phys. Rev. A* **103**, L061101 (2021).
- [50] G. S. J. Armstrong, D. D. A. Clarke, J. Benda, J. Wragg, A. C. Brown, and H. W. van der Hart, Enhancing spin polarization using ultrafast angular streaking, *Phys. Rev. A* **103**, 053123 (2021).
- [51] S. Walker, L. Kolanz, J. Venzke, and A. Becker, Selectivity in electron emission induced by ultrashort circularly polarized laser pulses, *Phys. Rev. Res.* **3**, 043051 (2021).
- [52] Y. Zhao, Y. Zhou, Q. Ke, J. Liang, Y. Liao, M. Li, and P. Lu, Resonance-induced ionization enhancement and suppression of circular states of the hydrogen atom in strong laser fields, *Phys. Rev. A* **104**, 032820 (2021).
- [53] T. F. Jiang, Photoelectron spectra of argon in circularly polarized pulses studied by atom-Volkov strong-field approximation, *J. Phys. B: At. Mol. Opt. Phys.* **55**, 075601 (2022).
- [54] L.-C. Wen, W.-Q. Jing, C.-P. Sun, X.-H. Gao, Z.-H. Jiao, G.-L. Wang, J.-H. Chen, and S.-F. Zhao, Role of excitation in the electron rotational asymmetry in circularly polarized laser fields, *J. Phys. B: At. Mol. Opt. Phys.* **56**, 125601 (2023).
- [55] D. Ikeya, H. Fujise, S. Inaba, M. Takahashi, M. Yamamoto, T. Nakamura, Y. Nagao, A. Matsuda, M. Fushitani, and A. Hishikawa, Orbital effects on tunnel-electron momentum distributions: Ar and H_2 studied by electron-ion coincidence momentum imaging, *J. Electron Spectrosc. Relat. Phenom.* **262**, 147280 (2023).
- [56] M. Han, P. Ge, Y. Fang, and Y. Liu, Wavelength scaling of photoionization circular dichroism of atomic electron ring currents and its effect on photoelectron spin polarization, *Phys. Rev. A* **107**, 063104 (2023).
- [57] A. N. Artemyev, E. Kutscher, B. M. Lagutin, and P. V. Demekhin, Theoretical study of spin polarization in multiphoton ionization of Xe, *J. Chem. Phys.* **158**, 154115 (2023).
- [58] U. Fano, Spin orientation of photoelectrons ejected by circularly polarized light, *Phys. Rev.* **178**, 131 (1969).
- [59] G. Baum, M. S. Lubell, and W. Raith, Spin-orbit perturbation in heavy alkali atoms, *Phys. Rev. Lett.* **25**, 267 (1970).
- [60] U. Heinzmann, J. Kessler, and J. Lorenz, Wavelength dependence of the Fano effect, *Phys. Rev. Lett.* **25**, 1325 (1970).
- [61] N. A. Cherepkov, Angular distribution and spin orientation of photoelectrons ejected by circularly polarized light, *Phys. Lett. A* **40**, 119 (1972).
- [62] P. Eckle, A. N. Pfeiffer, C. Cirelli, A. Staudte, R. Dörner, H. G. Müller, M. Büttiker, and U. Keller, Attosecond ionization and tunneling delay time measurements in helium, *Science* **322**, 1525 (2008).
- [63] A. N. Pfeiffer, C. Cirelli, M. Smolarski, D. Dimitrovski, M. Abu-samha, L. B. Madsen, and U. Keller, Attoclock reveals natural coordinates of the laser-induced tunnelling current flow in atoms, *Nat. Phys.* **8**, 76 (2012).
- [64] A. S. Landsman, M. Weger, J. Maurer, R. Boge, A. Ludwig, S. Heuser, C. Cirelli, L. Gallmann, and U. Keller, Ultrafast resolution of tunneling delay time, *Optica* **1**, 343 (2014).
- [65] L. Torlina, F. Morales, J. Kaushal, I. Ivanov, A. Kheifets, A. Zielinski, A. Scrinzi, H. G. Müller, S. Sukiasyan, M. Ivanov,

- and O. Smirnova, Interpreting attoclock measurements of tunnelling times, *Nat. Phys.* **11**, 503 (2015).
- [66] U. S. Sainadh, H. Xu, X. Wang, A. Atia-Tul-Noor, W. C. Wallace, N. Douguet, A. Bray, I. Ivanov, K. Bartschat, A. Kheifets, R. T. Sang, and I. V. Litvinyuk, Attosecond angular streaking and tunnelling time in atomic hydrogen, *Nature (London)* **568**, 75 (2019).
- [67] D. Trabert, N. Anders, S. Brennecke, M. S. Schöffler, T. Jahnke, L. Ph. H. Schmidt, M. Kunitski, M. Lein, R. Dörner, and S. Eckart, Nonadiabatic strong field ionization of atomic hydrogen, *Phys. Rev. Lett.* **127**, 273201 (2021).
- [68] Z. Xiao, W. Quan, S. Yu, X. Lai, X. Liu, Z. Wei, and J. Chen, Nonadiabatic strong field ionization of noble gas atoms in elliptically polarized laser pulses, *Opt. Express* **30**, 14873 (2022).
- [69] G. Kim, C. Hofmann, A. S. Maxwell, and C. Figueira de Morisson Faria, Twisted quantum interference in photoelectron holography with elliptically polarized fields, *Phys. Rev. A* **106**, 043112 (2022).
- [70] N. Douguet and K. Bartschat, Photoelectron momentum distributions in the strong-field ionization of atomic hydrogen by few-cycle elliptically polarized optical pulses, *Phys. Rev. A* **106**, 053112 (2022).
- [71] Y. Liu, W. Xie, M. Li, C. Cao, Y. Zhou, and P. Lu, Nonadiabatic tunneling ionization of atoms in few-cycle elliptically polarized laser pulses, *J. Phys. B: At. Mol. Opt. Phys.* **56**, 105601 (2023).
- [72] M. Yu Ivanov, M. Spanner, and O. Smirnova, Anatomy of strong field ionization, *J. Mod. Opt.* **52**, 165 (2005).
- [73] M. Klaiber, K. Z. Hatsagortsyan, and C. H. Keitel, Tunneling dynamics in multiphoton ionization and attoclock calibration, *Phys. Rev. Lett.* **114**, 083001 (2015).
- [74] R. Reiff, T. Joyce, A. Jaroń-Becker, and A. Becker, Single-active electron calculations of high-order harmonic generation from valence shells in atoms for quantitative comparison with TDDFT calculations, *J. Phys. Commun.* **4**, 065011 (2020).
- [75] B. H. Brandsen and C. J. Joachain, *Physics of Atoms and Molecules* (Addison-Wesley, Boston, 2003).